Macromolecules
ARTICLE

Macromolecules **2010**, *43*, 1261–1269 **1261**
DOI: 10.1021/ma902273s

Anthracene Based Conjugated Polymers: Correlation between $\pi-\pi$-Stacking Ability, Photophysical Properties, Charge Carrier Mobility, and Photovoltaic Performance

Daniel A. M. Egbe,*[,†,‡,§] Stefan Türk,[§] Silke Rathgeber,[⊥] Florian Kühnlenz,[∥] Rupali Jadhav,[†,∥] Andreas Wild,[#] Eckhard Birckner,[▽] Getachew Adam,[†] Almantas Pivrikas,[†] Vera Cimrova,[○] Günther Knör,[‡] Niyazi S. Sariciftci,[†] and Harald Hoppe*[,∥]

[†]*Linz Institute for Organic Solar Cells (LIOS), Johannes Kepler University Linz, Altenbergerstrasse 69, 4040 Linz, Austria,* [‡]*Institut für Anorganische Chemie, Johannes Kepler Universität Linz, Altenbergerstrasse 69, 4040 Linz, Austria,* [§]*Institute for Print and Media Technology, Chemnitz University of Technology, Reichenhainer Strasse 70, 09126 Chemnitz, Germany,* [⊥]*Institute of Physics, Johannes Gutenberg University Mainz, Staudingerweg 7, 55128 Mainz, Germany,* [∥]*Institute of Physics, Ilmenau University of Technology, Weimarer Strasse 32, 98693 Ilmenau, Germany,* [#]*Institut für Organische Chemie und Makromolekulare Chemie der Friedrich-Schiller Universität Jena, Humboldtstrasse 10, 07743 Jena, Germany,* [▽]*Institut für Physikalische Chemie der Friedrich-Schiller Universität Jena, Lessingstrasse 10, 07743 Jena, Germany, and* [○]*Institute of Macromolecular Chemistry, Academy of Sciences of the Czech Republic, Heyrovský Square 2, 162 06 Prague 6, Czech Republic*

Received October 15, 2009; Revised Manuscript Received December 11, 2009

ABSTRACT: This article reports on the synthesis, characterization and properties of a series of anthracene−containing poly(*p*-phenylene-ethynylene)-*alt*-poly(*p*-phenylene-vinylene)s (PPE−PPV) copolymers with general constitutional unit (Ph−C≡C−Anthr−C≡C−Ph−CH=CH−Ph−CH=CH−)$_n$ denoted **AnE-PV**. Solely linear (**AnE-PV*aa***, ***-ad***, ***-ae***) and solely branched (**AnE-PV*bb***) as well as mixed linear and branched (**AnE-PV*ab***, ***-ac***, ***-ba***, ***-cc***) alkoxy side chains were grafted to the backbone in order to tune the $\pi-\pi$-stacking ability of the materials. It has been possible to establish a correlation between $\pi-\pi$-stacking ability, absorptive behavior, charge carrier mobility, solar cell active layer nanoscale morphology and resulting photovoltaic performance. Solar cells energy conversion efficiencies between 0.34% and 3.14% were achieved. The best performance was achieved from **AnE-PV*ab*** showing both stacking ability and highest $\pi-\pi$-stacking distance of 0.386 nm as compared to 0.380 nm for the others. Poorer performance resulted from polymers with no inclination to stack, **AnE-PV*ba***, ***-bb***, although they exhibited the higher charge carrier mobilities. Hole mobilities range from 1.5×10^{-5} cm^2/V.s (**AnE-PV*ad***) to 4.5×10^{-4} cm^2/V.s (**AnE-PV*ba***). An increase of the open circuit voltage from ∼650 mV to ∼900 mV is observed with decreasing side chain density. In case of the **AnE-PV*cc***:PCBM (1:1) blend a 2-fold increase in solar cell efficiency (from 1% to 2%) was obtained when the active layer was spin cast from a 1:1 mixture of chloroform:chlorobenzene instead of using chlorobenzene.

Introduction

The need and desire to develop cheap renewable energy sources have triggered worldwide intensive research for efficient, flexible, low cost and lightweight photovoltaic devices based on organic semiconducting materials.[1,2] Among the various types of organic photovoltaic cells, polymer-fullerene bulk heterojunction (BH) solar cells are by far the most successful with certified power conversion efficiencies above 6%.[3] The nanoscale morphology of the active layer is a key parameter for the design of high performance polymer−fullerene bulk heterojunction solar cells. An optimized active layer should combine the following requirements: (1) high contact area between donor and acceptor, (2) a good match of HOMO and LUMO energy positions of both components, that guarantees an efficient dissociation of the photogenerated excitons into free charge carriers at the interface, and (3) an efficient percolating path for both electron and hole to the corresponding electrodes.[2] Ways to improve the solar cell performance by tuning the morphology of the active layer have been described in the literature. These include the use of specific solvents or solvents mixtures for film deposition,[4] annealing[5] and changing the drying conditions of the active layers as well as the use of additives.[6] For instance an improvement of the energy conversion efficiency, $\eta_{AM1.5}$, was observed when the solvent used for spin coating deposition of the active layers was changed from toluene to chlorobenzene,[4] Annealing P3HT (poly(3-hexylthiophene))-PC$_{61}$BM (6,6-phenylC$_{61}$-butyric acid methylester) solar cells substantially enhances their performance as compared to their non annealed counterparts.[5] Heeger et al. observed an improvement of $\eta_{AM1.5}$ by a factor of 2 (from 2.8% to 5.5%) by using octane-dithiol as processing additive for morphology control in PCPDTBT (poly[2,6-(4,4-bis(2-ethylhexyl)-4*H*-cyclopenta[2,1-*b*;3,4-*b*′]-*alt*-4,7-(2,1,3-benzothiadiazole)])-PC$_{71}$BM(6,6-phenyl-C$_{71}$butyric acid methyl ester) bulk heterojunction solar cells.[6]

On the basis of poly(arylene-ethynylene)-*alt*-poly(arylene-vinylene)s PAE−PAVs,[7] we were able to demonstrate that the solubilizing alkoxy side chains are a further significant aspect to be considered in the control of the active layer nanomorphology as a result of their hydrophobic nature.[8,9] Electrochemical studies yield that alkyl side groups act as a shield around the conjugated

*To whom correspondence should be addressed. E-mail: (D.A.M.E.) daniel_ayuk_mbi.egbe@jku.at; (H.H.)harald.hoppe@tu-ilmenau.de.

Published on Web 01/04/2010

Scheme 1. Synthesis of Anthracene-Containing Polymers AnE-PV

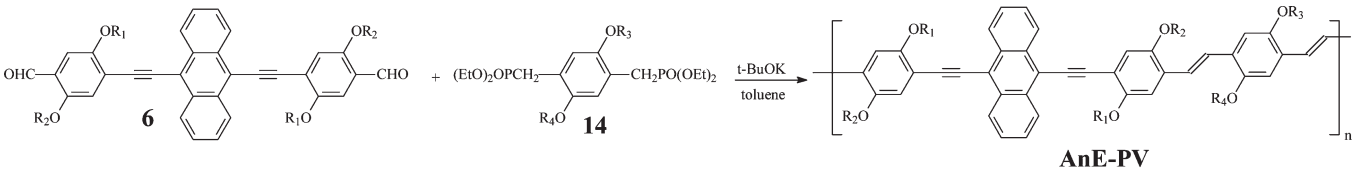

AnE-PV

AnE-PV	R_1	R_2	R_3	R_4
aa	octyl	octyl	octyl	octyl
ad	octyl	octyl	decyl	decyl
ae	octyl	octyl	dodecyl	dodecyl
af [13a]	octyl	octyl	octadecyl	octadecyl
ab	octyl	octyl	2-ethylhexyl	2-ethylhexyl
ac	octyl	octyl	methyl	2-ethylhexyl
cc	methyl	2-ethylhexyl	methyl	2-ethylhexyl
ba	2-ethylhexyl	2-ethylhexyl	octyl	octyl
bb	2-ethylhexyl	2-ethylhexyl	2-ethylhexyl	2-ethylhexyl

backbone and thus hinder the transfer of charges.[8,10] Very high side chain density is disadvantageous in the construct of solar cells due to the following reasons: (1) they dilute the concentration of the absorbing conjugated species per volume unit, so that less photons are absorbed, and (2) they reduce the interfacial area between donor and acceptor components leading to strong phase separation and concomitant poor photovoltaic performance. On the other hand, the nature (linear or branched) and length of the alkoxy side chains can be useful in the control of the $\pi-\pi$-stacking of rigid conjugated polymers and their photoluminescent behavior.[11] Strong $\pi-\pi$-stacking (synonymous to small $\pi-\pi$-stacking distance) generally leads to broadening of the photoluminescence spectra and quenching of the fluorescence attributed to excimer formation.[12]

This paper is dedicated to a series of anthracene-containing PAE−PAVs of general constitutional unit: (Ph−C≡C−Anthr−C≡C−Ph−CH=CH−Ph−CH=CH−)$_n$, (**AnE-PV**) in which the nature and length of the side chains as well as the side chain density has been varied in a systematic manner in order to tune the nanomorphology of the active layers by means of changing the $\pi-\pi$-stacking ability and, thus, the photovoltaic performance. Solely linear (**AnE-PV*aa***, **-*ad***, **-*ae***) and solely branched (**AnE-PV*bb***) as well as mixed linear and branched (**AnE-PV*ab***, **-*ac***, **-*ba***, **-*cc***) alkoxy side chains were grafted to the backbone. In the polymer **AnE-PV*ac*** and **-*cc*** the side chain density is reduced compared to the polymers **AnE-PV*ab*** and **-*bb*** by partly replacing the branched side chains by methyl groups. Two polymers of this type, one of this series, **AnE-PV*ab***, and another one bearing octadecyloxy side groups at R_3 and R_4 (see Scheme 1), **AnE-PV*af***, have been investigated before.[13,14] It has been shown that the presence of the electron rich anthracenylene units within the backbone lowers the optical and electrochemical band gap energies compared to MDMO-PPV,[13,14] making these materials viable for solar cell applications. Furthermore, the absorbance is increased in the **AnE-PV*ab***:PCBM active layers compared to the **MDMO-PPV**:PCBM counterparts. In ref 14 a power conversion efficiency of 2% was attained, which is less than the value of 3.14% achieved for **AnE-PV*ab*** in the present work. This difference might be ascribed to differences in molecular-weights, as has been demonstrated by Schilinsky et al.[1b] as well as differences in the experimental conditions. **AnE-PV*ab*** also served as donor material in polymer-Vinazene (a derivative of 2-vinyl-4,5-dicyanoimidazole) bulk heterojunctions solar cells.[15] Solar cell efficiencies did not exceed 0.42% in that case.

The goal of the present study is to draw conclusions about the correlation between side chain substitution, the nanoscale morphology and in particular the $\pi-\pi$-stacking ability, the photophysical properties (absorption, emission, absolute fluorescence quantum yield), the intrinsic charge carrier mobility, as determined by the CELIV (charge extraction by linearly increasing voltage) measurement technique, and the photovoltaic performance. The $\pi-\pi$-stacking distance was determined by means of wide-angle X-ray scattering performed on extruded filaments.[16] Electrochemical studies have been carried out in order to estimate the HOMO and LUMO-levels as well as the band gap energies.

Results and Discussion

Synthesis and Characterization. The polymers were synthesized by reaction of dialdehydes **6** with bisphosphonate esters **14**[11b,c,19] based on well established protocols (see Scheme 1).[9,17−20] The synthetic paths leading to the starting materials (**6** and **14**) are depicted in the Supporting Information (Schemes S1 to S3). Soluble materials were obtained with yields between 50% and 90% after extraction of the products with hot diethyl ether. Solely linear (**AnE-PV*aa***, **-*ad***, **-*ae***), solely branched (**AnE-PV*bb***) as well as mixed linear and branched (**AnE-PV*ab***, **-*ac***, **-*ba***, **-*cc***) alkoxy side chains were grafted to the backbone. In the polymer **AnE-PV*ac*** and **-*cc*** the side chain density is reduced compared to the polymers **AnE-PV*ab*** and **-*bb*** by partly replacing the branched side chains by methyl groups. All the polymers except **AnE-PV*aa*** and **-*ac*** are soluble in common organic solvents such as chloroform, dichloromethane, tetrahydrofuran (THF), toluene and chlorobenzene. The chemical structures of the materials were confirmed by ^{1}H NMR, ^{13}C NMR, IR and elemental analysis.[13a,14a] Results obtained from GPC (THF as eluent, polystyrene standards) and thermogravimetric analysis (TGA) as well as yields of the materials are provided in Table 1. TGA curves of the polymers are provided as Supporting Information (Figure S1).

Structural Studies. Wide-angle X-ray scattering (WAXS) measurements have been performed on the powder samples as well as on aligned fiber samples in order to obtain information about the nanomorphology of the polymer materials. The determination of the $\pi-\pi$ stacking distance ($d_{\pi\pi}$) was done as described in detail in ref 16b. The polymers bearing linear octyl side chains at R_1 and R_2 (**AnE-PV*aa***, **-*ad***, **-*ae***, **-*ab***, **-*ac***) arrange in a layered structure (see Scheme 1) that involves $\pi-\pi$-stacking (distance $d_{\pi\pi}$) of the conjugated backbones and layered ordering of the conjugated backbones separated by the side chains perpendicular to the

Table 1. Yields, GPC (THF as eluent, polystyrene standards) and TGA of AnE-PV[a]

AnE-PV	yield (%)	M_n (g/mol)	M_w (g/mol)	PDI	DP	$T_{5\%}$ (°C)	$T_{10\%}$ (°C)	$d_{\pi\pi}$ (nm)
aa						326	343	0.380
ad	90	19 300	54 000	2.79	15	330	351	0.380
ae	82	13 300	26 200	1.97	10	338	364	0.380
ab	83	40 000	141 600	3.54	32	306	317	0.386
ac						322	348	0.381
cc	86	47 500	91 900	1.9	48	309	317	0.379
								0.344
ba	53	25 500	77 800	3.05	20	327	348	
bb	94	15 800	47 200	2.98	13	325	346	

[a] M_n = number-average molecular weight, M_w = weight-average molecular weight, PDI = polydispersity index, DP = degree of polymerization, $T_{5\%,10\%}$ = decomposition temperatures at 5% and 10% weight loss, respectively. $d_{\pi\pi}$ = $\pi-\pi$-stacking distance (the values are given with an error of ±0.002 nm).[16b]

$\pi-\pi$-stacking direction. The asymmetric substituted polymer **AnE-PV*cc*** is amorphous in the as synthesized sample but it also arranges in a stacked structure when it is annealed above ≈210 °C, i.e., above the backbone reorganization temperature. In contrast, polymers with 2-ethylhexyl substitution at R_1 and R_2, i.e., close to the anthracenylene−ethynylene moiety are amorphous. No $\pi-\pi$-stacking is observed for these polymers. Both compounds exhibited poorer photovoltaic performance compared to the other polymers in this series. Table 1 summarizes the $\pi-\pi$-stacking distances, $d_{\pi\pi}$, obtained for the nonamorphous samples from the WAXS fiber spectra. For polymers bearing solely linear side chains, **AnE-PV*aa***, **-*ad***, **-*ae***, as well as the polymer having asymmetric side chains at R_3 and R_4, **AnE-PV*ac***, the $\pi-\pi$-stacking distance was determined to be 0.380 nm. For the asymmetric substituted polymer **AnE-PV*cc*** two peaks were observed in the WAXS spectra which correspond to $\pi-\pi$-stacking distances of about 0.380 nm (as for the polymers **AnE-PV*aa***, **-*ad***, **-*ae***, **-*ac***) and 0.344 nm, respectively. The appearance of two peaks might be due to the presence of two polymorphs. The grafting of bulky, branched 2-ethylhexyl at R_3 and R_4 in **AnE-PV*ab*** widens the stacking distance to 0.386 nm. This widening leads to better photovoltaic performance as reported below.

Photophysical Investigations. The photophysical data of the polymers as well as those of their starting materials were measured in chloroform solution as well as in thin films spin coated from chloroform and chlorobenzene, respectively (see Table 2). Results include the wavelength (λ) at the absorption maximum, λ_a, λ at which 10% of the absorption maximum is reached on the lower energy side, $\lambda_{a10\%}$, the optical band gap energy calculated using $1240/\lambda_{a10\%}$, E_g^{opt},[13a] the wavelength at the emission maximum, λ_f, the Stokes shift, $\Delta\nu_{af}$, as well as the relative and absolute fluorescence quantum yield, Φ_f.

Figure 1 depicts the absorption and emission spectra in dilute chloroform solution. Already in solution, polymers bearing solely linear side chains, **AnE-PV*i*** (*i* = ***ad***, ***ae***, and ***af***[13a]), and those incorporating branched 2-ethylhexyl, **AnE-PV*i*** (*i* = ***ab***, ***ba***, ***bb***, and ***cc***) show distinct behavior. The absorption spectra of the first group exhibit a shoulder around 600 nm, which is ascribed to the formation of aggregates already in dilute medium (Figure 1, left). This is confirmed by recording temperature-dependent absorption spectra of **AnE-PV*ad*** in toluene (see Figure 2). The shoulder band gradually disappears upon temperature increase from 20 to 80 °C coupled with a blue shift of the absorption peak from 540 to 528 nm. Subsequent cooling from 80 to 20 °C results in an increase of the intensity and a red shift (λ_a = 544 nm) of the main absorption peak, with a final transformation of the shoulder band to a real peak centered at 596 nm with enhanced intensity. This is an evidence of an enhanced backbone planarization and stronger intermolecular interactions (aggregation) induced by the cooling process. This heating and cooling process might be useful to induce preorganization of polymers prior to the spin-coating step during solar cell preparation.

Table 2. Photophysical Data of the Dialdehydes 6 and Polymers AnE-PV[a]

code		λ_a (nm)	$\lambda_{a10\%}$ (nm)	E_g^{opt} (eV)	λ_f (nm)	$\Delta\nu_{af}$ (cm^{-1})	Φ_f (%)
			Monomers				
6a	1	512	520	2.38	524	450	80
6b		511	532	2.33	525	520	84
6c		510	530	2.33	524	520	86
			AnE-PV Polymers				
ad	1	545	608	2.03	578	1050	51
	2	544, 583	624	1.98	623, 673	1100	2
	3	552, 590	650	1.91	621	850	
ae	1	540	604	2.05	577	1190	38
	2	550, 580	638	1.94	623	2130	4
	3	539, 577	625	1.98	605	2020	
ab	1	546	584	2.12	579	1050	50
	2	541, 570	622	1.99	622	2400	2
	3	508, 583	687	1.80	624	1100	
cc	1	544	580	2.13	578	1080	60
	2	540, 578	628	1.97	617	2300	2
	3	532, 580	674	1.84	617	2590	
ba	1	510	575	2.15	576	2250	24
	2	507	596	2.08	602	3100	3
	3	504	636	1.95	605	3300	
bb	1	519	578	2.14	580	2030	45
	2	521	610	2.03	598	2470	6
	3	527	613	2.02	600	2300	

[a] Key: (1) in chloroform solution and films spin coated from (2) chloroform and (3) chlorobenzene, respectively; λ_a (wavelength λ at absorption maximum); $\lambda_{a10\%}$ (λ at 10% of the absorption maximum on the lower energy side); E_g^{opt} (optical band gap energy calculated using $1240/\lambda_{a10\%}$), λ_f (λ at emission maximum), $\Delta\nu_{af}$ (Stokes shift) and Φ_f (fluorescence quantum yield measured relative to rhodamine 6G for solutions and absolute values from intergrating sphere for thin film samples).

The absorption peak of the polymers **AnE-PV*i*** (*i* = ***ba***, λ_a = 510 nm; *i* = ***bb***, λ_a = 519 nm) bearing bulky 2-ethylhexyl at R_1 and R_2, i.e. close to the AnE unit, is blue-shifted relative to that $\lambda_a\sim$ 545 nm of the polymers **AnE-PV*i*** (*i* = ***ad***, ***ae***, ***af***,[13a] ***ab***) bearing linear side chains ($R_1 = R_2$ = octyl) and the asymmetric substituted polymer **AnE-PV*cc*** (R_1 = 2-ethylhexyl, R_2 = methyl). This hypsochromic shift is due to the high sensitivity of the anthracene moiety to steric hindrances in its neighborhood, as was previously demonstrated by others[21] and by us.[13b] In the polymer **AnE-PV*cc*** the small

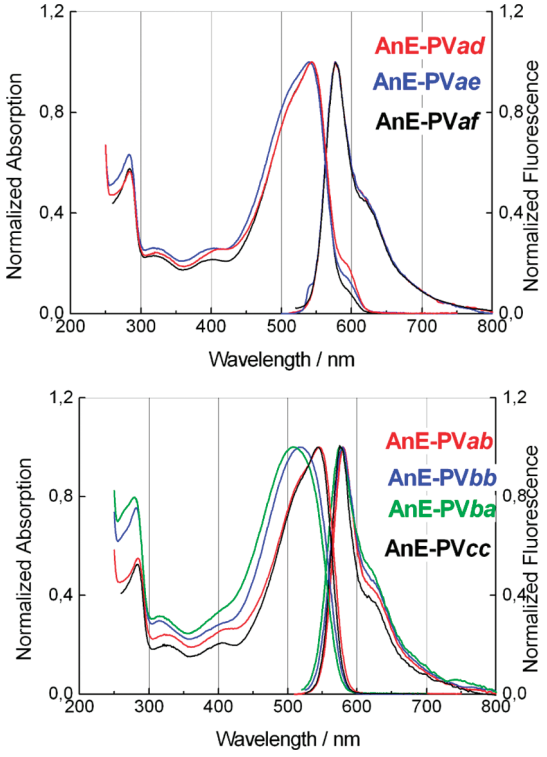

Figure 1. Absorption and emission spectra in dilute chloroform solution.

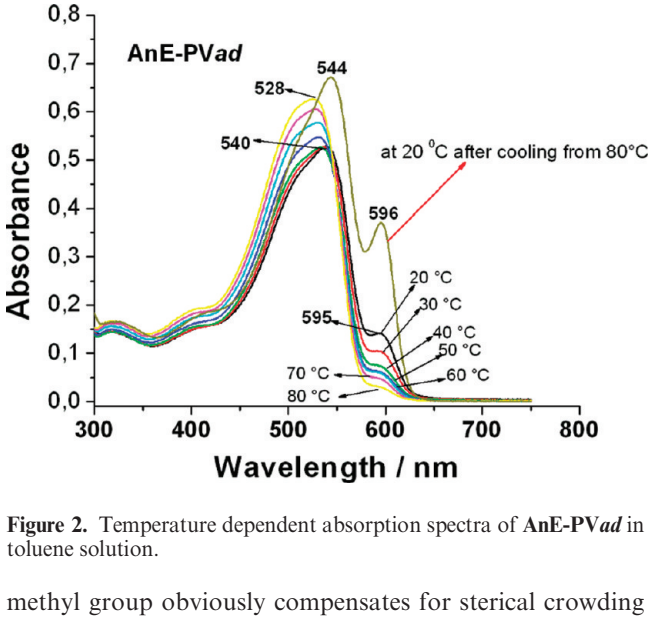

Figure 2. Temperature dependent absorption spectra of **AnE-PV*ad*** in toluene solution.

methyl group obviously compensates for sterical crowding induced by the bulky 2-ethylhexyl group at R_2.

Despite the differences in the solution absorptive behavior resulting in optical band gap energies between 2.0 and 2.1 eV, the main emission peak for all polymers in solution (i.e.$S_{10} \rightarrow S_{00}$ transition) is centered around $\lambda_f = 580$ nm. This leads to a Stokes shift, $\Delta\nu_{af}$, of approximately 1000 cm^{-1} for all polymers except for **AnE-PV*ba*** and -***bb***. The latter polymers exhibit 2-fold higher Stokes shifts, suggesting a stronger conformational change between the ground state S_0 and the first excited state S_1. Moreover, both materials show the highest ratio between the intensities of the $S_{10} \rightarrow S_{01}$ and $S_{10} \rightarrow S_{00}$ transitions (Figure 1, right). This is an indication for a less rigid planar S_1 state, which might also explain the lowest quantum yield ($\Phi_f = 24\%$) of **AnE-PV*ba***. All the other polymers exhibit in solution Φ_f values between 40 and 60%, which are lower than those of their more rigid monodisperse starting materials **6** ($\Phi_f = 80-86\%$).

Table 3. Data Obtained from Fluorescence Kinetics Studies in Chlorobenzene Solutions[a]

AnE-PV	$\Phi_{f\ chloroform}$ (%)	$\Phi_{f\ chlorobenzene}$ (%)	τ (ns)	k_f (ns^{-1})	k_{nr} (ns^{-1})
ad	51	28	1.00	0.28	0.72
ae	38	49	0.96	0.30	0.53
ab	50	57	0.94	0.61	0.46
ac		55	0.99	0.56	0.45
cc	60	62	0.92	0.67	0.41
ba	24	29	0.72	0.40	0.99
bb	45	48	0.85	0.56	0.61

[a] Fluorescence quantum yield measured relative to rhodamine 6G, Φ_f, fluorescence lifetimes, τ, and rate constants of radiative, k_f, and nonradiative deactivation, k_{nr}.

Results obtained from fluorescence kinetics studies measured in chlorobenzene are summarized in Table 3. This includes the fluorescence lifetime, τ, the radiative deactivation constant, k_f, and the nonradiative deactivation constant, k_{nr}, together with the fluorescence quantum yield Φ_f. These results reveal no significant differences in the solution deactivation processes for all polymers except for compounds **AnE-PV*ad*** and ***ba***; which exhibit the lowest fluorescence quantum yield, $\Phi_f = 28\%$ and 29%, and the highest nonradiative deactivation constants, $k_{nr} = 0.72$ ns^{-1} and 0.99 ns^{-1}, respectively. The remarkable fluorescence quenching in both cases could be attributed in the case of **AnE-PV*ad*** to the stronger aggregate formation in aromatic solvents (promoting $\pi-\pi$-stacking as in the case of toluene, compare Figure 1 left with Figure 2) than in chloroform and, in the case of **AnE-PV*ba*** to a less planarized excited state, as already mentioned above.

Figure 3 shows the absorption and emission spectra of the pristine polymer thin films of **AnE-PV*ad***, ***ab***, ***ba***, and ***cc*** and of the corresponding polymer−PCBM active layers (weight ratio 1:1). The films were spin-cast from chlorobenzene. There is substantial photoluminescence quenching in the blend due to photoinduced charge transfer from the polymer to PCBM.[1,2] From the absorption spectra, the polymer can be divided into two main groups: (1) polymers bearing solely linear side chains close to the AnE units (i.e., $R_1 = R_2$ = octyl), **AnE-PV*i*** (i = ***ad***, ***ae***, ***ab***) and (2) polymers having solely bulky branched 2-ethylhexyl at R_1 and R_2, **AnE-PV*i*** (i = ***ba***, ***bb***). The first group shows well resolved absorption spectra, with main absorption bands consisting of two peaks around 540 and 580 nm. The appearance of two peaks is evidence of improved ordering as confirmed by X-ray scattering investigations from which the intermolecular $\pi-\pi$-stacking distance $d_{\pi-\pi}$ and interlayer stacking distance were determined. In contrast, the $\pi-\pi^*$ transition band of the second group is structureless. This finding is in accordance with the X-ray findings results revealing that these polymers are in the amorphous state, i.e. no $\pi-\pi$-stacking signal and no interlayer ordering were observed. The absorption peak of these polymers is located around 505 and 520 nm for **AnE-PV*ba*** and **AnE-PV*bb***, respectively. The polymer **AnE-PV*cc*** bearing a small methyl- as well as a branched 2-ethylhexyl group close to AnE shows an intermediate behavior. The absorption band of **AnE-PV*cc*** is slightly structured in the pristine form, but becomes structureless in the blend.

For the optical band gap energies, E_g^{opt}, lower values were obtained for thin films as compared to the solutions due to enhanced planarization and intermolecular interaction in the films (see Table 2). Films spin-cast from

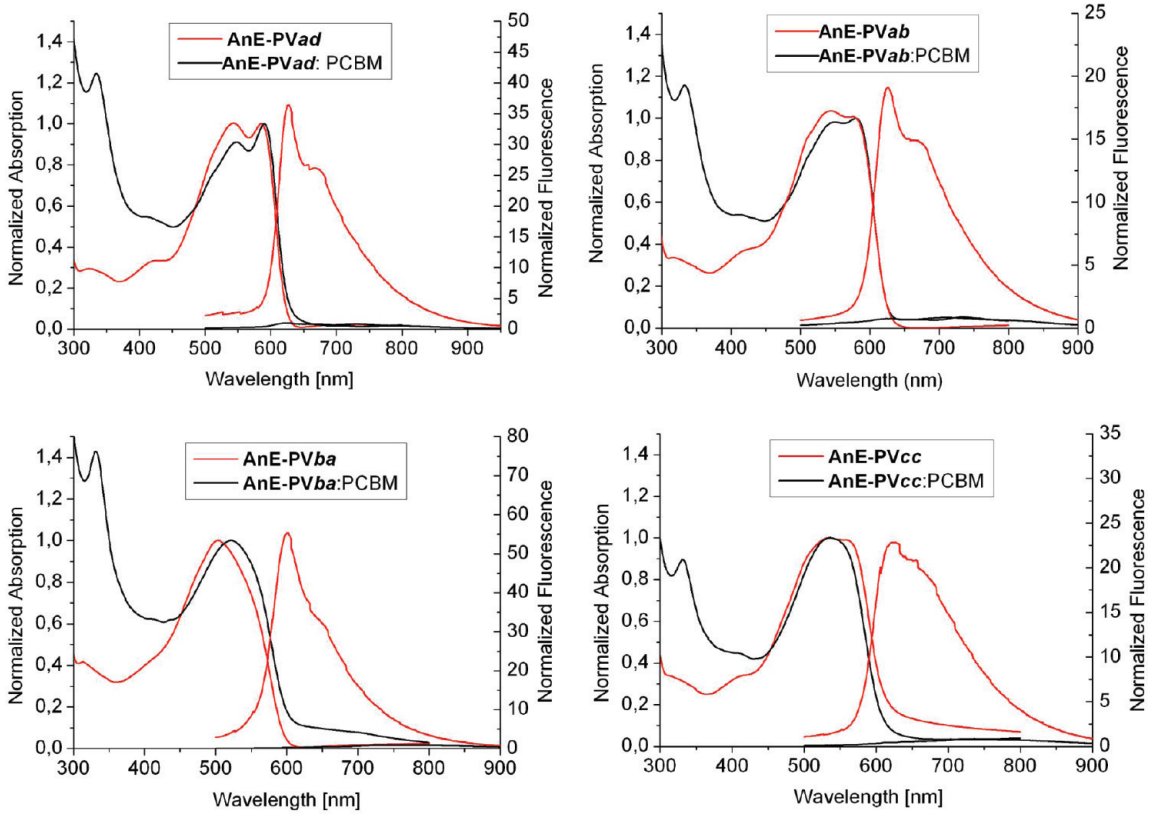

Figure 3. Thin film absorption and emission spectra are shown for polymers **AnE-PV*ad***, ***-ab***, ***-ba***, and ***-cc***, and their 1:1 blends with PCBM. The films were spin-cast from chlorobenzene.

Table 4. Electronic Data Obtained for Polymer Films Spin-Cast from Chlorobenzene[a]

AnE-PV	HOMO (eV)	LUMO (eV)	E_g^{elc} (eV)	E_g^{opt} (eV)	ΔE_g (eV)
ad	5.15	3.38	1.77	1.91	0.14
ae	5.14	3.36	1.78	1.98	0.20
ab	5.17	3.37	1.80	1.80	0.00
cc	5.15	3.34	1.81	1.84	0.03
ba	5.16	3.37	1.79	1.95	0.16
bb	5.19	3.40	1.79	2.02	0.23

[a] Optical band gap energies E_g^{opt} were taken from Table 2 for comparison purpose.

chlorobenzene solution are in general characterized by lower E_g^{opt} values than those obtained from chloroform. This is due to the fact that non aromatic solvents, such as chloroform, tetrahydrofuran or dichloromethane, prefer to interact with the alkoxy side chains, while aromatic solvents are known to interact preferentially with the aromatic rings, causing the polymers chains to lie open and flat, thus enhancing the backbone planarization.[22] Optical band gap values are in the range of 1.8 and 2.0 eV, the lower end being similar to the electrochemical ones (see below and Table 4). This variation of E_g^{opt} values might be related to differences in backbone coplanarity and film thickness.[9a] As expected, lower absolute fluorescence quantum yields between 2% and 6% were obtained in thin film as compared to the solution. **AnE-PV*bb*** gave the highest value, possibly due to hindered $\pi-\pi$ stacking resulting from grafting of solely bulky branched 2-ethylhexyl. It is, however, difficult to make a clear structure−property relation based on the obtained absolute Φ_f values, conscious of the fact that absolute photoluminescence quantum yields are obtained with a broad margin of error, due to the intrinsic difficulties of the method.

Electrochemical Studies. Measurements were performed on thin polymer films spin coated from chlorobenzene solutions under strictly inert conditions.[13b] The ionization potential (HOMO level), E_{IP}, and electron affinity (LUMO level), E_A, were estimated from oxidation and reduction onset potentials on the basis of the reference energy level of ferrocene (4.8 eV below the vacuum level) using the equation $E_{IP}(E_A) = -(E_0 - E_{ferr}) - 4.8$ eV, where E_{ferr} is the value for ferrocene vs the Ag/Ag^+ electrode. E_0 values were obtained averaging the anodic and cathodic peak potentials, $E_0 = (E_{pa} + E_{pc})/2$. The E_{IP} and E_A values were evaluated from the first oxidation and reduction peaks of the cyclic voltamograms (CV) measured on several samples at scan rates of 20 and 50 mV/s. The CV curves are shown in the Supporting Informationn (Figure S2) and the electronic data are summarized in Table 4 (values for E_g^{opt} were included from Table 2 for comparison purpose). For the evaluation, usually the first two runs were taken. The electrochemical band gap energy, E_g^{elc} for all polymers is 1.80 eV. The difference, ΔE_g between E_g^{opt} and E_g^{elc} varies from 0 to 200 meV, which might be related, among other reasons, to differences in thin film preparation during the optical and electrochemical process resulting in differences in thin film thicknesses and concomitant backbone coplanarity.

Mobility Studies. It is a challenge to measure the charge carrier mobilities of solution processed organic semiconductors due to their disordered structure resulting in hopping transport within localized energy states and time-dependent dispersive charge transport.[23,24] The Charge Extraction by Linearly Increasing Voltage (CELIV) method has been used successfully to study the charge transport in various disordered organic and inorganic semiconducting films.[25] The main advantages of this method over time-of-flight (TOF) is that it allows to study films with various conductivities as

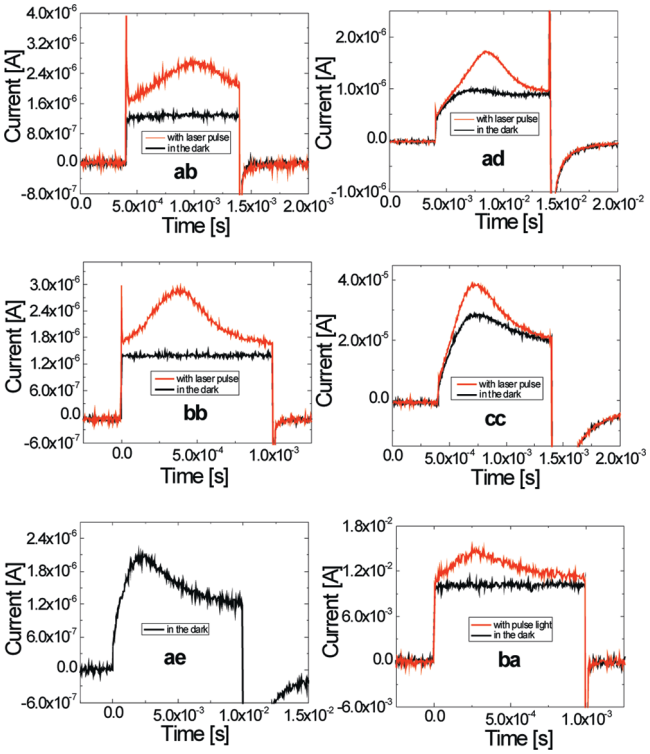

Figure 4. CELIV current transients are shown for all polymers studied. The charge carrier mobility was calculated from the extraction maxima using laser light pulse (top red curves in the figures) except for **AnE-PV*ae*** polymer where carrier mobility is measured in the dark. From the current transients recorded in the dark (bottom black curves in the figures) it is seen that **AnE-PV*ae***, **AnE-PV*cc***, and **AnE-PV*ad*** had unintentional doping which allows carrier mobility measurements even without laser pulse. The equilibrium carrier concentration and film conductivity has been calculated from these transients.

well as with rather dispersive charge transport.[26,27] In contrast to the application of planar organic field effect transistor (OFET) geometry it yields also information about the transport in the perpendicular direction to the substrate plane,[28] and contact resistance which often leads to incorrect carrier mobility values in OFET is not a problem.[29] The essence of this time-resolved method is that the triangle-shaped voltage pulse is applied to the sandwich-type film forming a capacitor with ITO and Al electrodes. If the film conductivity is low and no laser pulse is used for photogeneration, the current response to the applied pulse results in a constant displacement charging current $j(0)$ [see Supporting Information, Figure S3, bottom]. But if equilibrium of photogenerated charge exists in the film, it will contribute to the conductivity current in addition to the displacement current seen as an excess signal $\triangle j$. A laser pulse is used prior to the extracting triangle voltage pulse with a delay time t_{del} (see Supporting Information, Figure S3, top). A negative offset voltage is used to compensate for the built-in potential in the device, therefore restricting the charge carrier extraction during the delay time t_{del}. When no time-dependent carrier mobility is measured, t_{del} is chosen to be much shorter that t_{pulse}. During the carrier extraction, the photocurrent increases due to the fact that more carriers start to participate in the transport until the extraction maxima is reached. Subsequently the current decreases because the majority of all carriers have reached the back electrode. From the extraction of the maxima the carrier mobility as well as film conductivities are directly calculated using equations derived elsewhere.[30]

Table 5. Hole Mobility, μ_{hole}, of the Polymers Arranged in Increasing Order

AnE-PV	μ_{hole} [cm^2/(Vs)]
ad	1.69×10^{-5}
ab	2.57×10^{-5}
ae	3.39×10^{-5}
cc	9.22×10^{-5}
bb	1.53×10^{-4}
ba	4.52×10^{-4}

CELIV current transients were measured for all polymers and are presented in Figure 4. For all polymers except **AnE-PV*ae***, which shows high dark conductivity within given experimental conditions, the charge carriers were photogenerated with laser pulse. After 100 ns delay time, the applied triangle-shaped rising voltage pulse extracts the photogenerated charge carriers toward back electrode and the carrier mobility is directly estimated from the extraction maxima. Polymers **AnE-PV*ad***, ***-ae***, and ***-cc*** show extraction maxima even in the dark current transients, indicating the presence of equilibrium thermally generated charge carriers in the film due to unintentional doping. The film conductivities were calculated to be $\sigma = 1.3 \times 10^{-10}$ S/cm (**AnE-PV*ad***), $\sigma = 9 \times 10^{-9}$ S/cm (**AnE-PV*ae***), and $\sigma = 2.8 \times 10^{-9}$ S/cm (**AnE-PV*cc***) whereas the rest of the polymers show much lower level of doping as can be seen from flat dark current transients. For **AnE-PV*cc***, the extraction maximum positions are the same with laser pulse and in the dark i.e. the photogenerated carrier mobility is equal to the steady state equilibrium mobility. However, **AnE-PV*ad*** polymer shows delayed extraction maxima for photogenerated carriers, possibly due to space charge effects prolonging the extraction of the reservoir of photogenerated charge carriers.

Since the laser pulse was illuminating the positive electrode during the measurements, the photocurrent due to mobile holes is recorded and the mobility of photogenerated holes is calculated from the current transients. The values are summarized in Table 5. The values range from 1.5×10^{-5} cm^2/(Vs) (**AnE-PV*ad***) to 4.5×10^{-4} cm^2/(Vs) (**AnE-PV*ba***). In contrast to thiophene-based poly(arylene)s,[31] the amorphous polymers (**AnE-PV*bb***, ***-ba***), i.e. polymers bearing 2-ethylhexyl close to the AnE unit exhibit higher charge carrier mobilities than those with higher stacking tendency (**AnE-PV*ad***, ***-ae***, ***-ab***). This would suggest that $\pi-\pi$ stacking might be detrimental to charge carrier mobility for this class of compounds. Similar trends were previously observed in photoconductivity studies on PPE−PPV materials, whereby higher photoconductivity values detected at lower threshold voltages were obtained for materials with less aggregation tendency. Decreasing aggregation tendency were achieved through grafting of either very long linear octadecyl or bulky branched 2-ethylhexyl side chains laterally to the conjugated backbones.[9b,11c,13a] It was assumed that photoconductivity is more an intramolecular process than an intermolecular one.[13a] Similar conclusions might be valid for the **AnE-PV** polymers investigated here. However, further studies on other PPE−PPV based materials are necessary before a final conclusion can be drawn.

Morphological Studies. Polymer:PCBM (1:1) blends were spin-cast from chlorobenzene solutions on glass slides and their topography was investigated by tapping-mode atomic force microscopy (AFM) measurements in order to investigate the kind and scale of phase separation present within the photoactive layers. Figure 5 shows the AFM results. Polymers with linear side chains near the AnE units (**AnE-PV*ad***, ***-ae***, and ***-ab***) result in more coarse scale morphologies reflected by peak-to-valley variations between 10 and 20

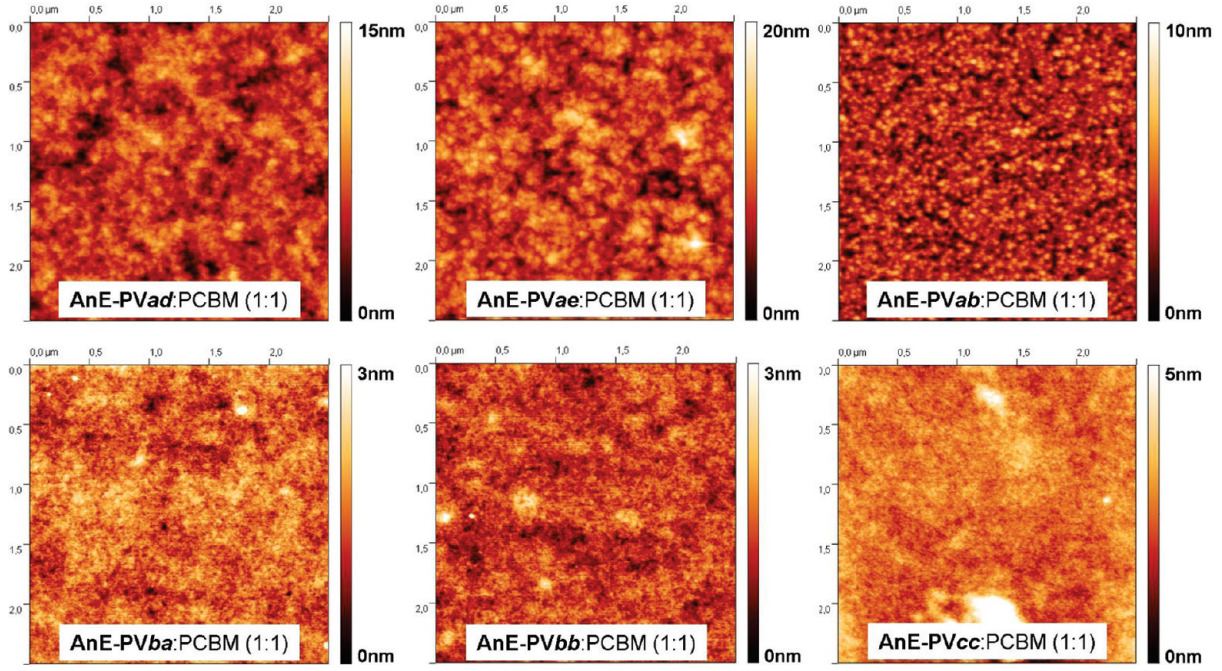

Figure 5. Tapping mode AFM images (area 2.5 × 2.5 μm^2) are shown for polymers **AnE-PV*ad***, ***-ae***, ***-ab***, ***-ba***, ***-bb***, and ***-cc***. Linear side chains near the AnE-unit result generally in more coarse scale morphologies, while branched groups lead to more intimate phase blending.

nm and by features indicating the formation of polymeric aggregates. On the other hand, polymers bearing branched side chains near the AnEunit (**AnE-PV*bb***, ***-ba***) result in fine scale morphologies resulting in rather flat topographies varying within only 3 nm. The thin film morphologies obtained for the asymmetrically substituted polymer **AnE-PV*cc*** are similar to that obtained for amorphous **AnE-PV*bb*** and ***-ba*** due to reduced side chain density. It seems that the higher crystallization tendency of the polymers **AnE-PV*ad***, ***-ae***, and ***-ab***, which for the polymers **AnE-PV*ad*** and ***-ae*** already results in preorganization in dilute solutions, leads to more coarse scale thin film morphologies of the polymer: PCBM blends. More coarse grained film morphologies directly result in improved photovoltaic behavior (see discussion below). This is probably due to improved percolation paths and, thus, better charge transport for both signs of charge carriers.

Photovoltaic Studies. All solar cells were prepared on glass substrates coated with indium tin oxide (ITO) according to the following standard procedure: part of the ITO was etched away in order to allow for nonshunting counter contacts at the aluminum electrode. In a second step a poly(3,4-ethylenedioxythiophene)−poly(styrenesulfonate) (PEDOT:PSS) film was spin-cast from aqueous solution and annealed at 180 °C for 15 min. Subsequently the active layer was spin-cast from chlorobenzene under inert atmosphere conditions. Afterward the layer stack was transferred into the vacuum chamber and a 100 nm thick aluminum back electrode was thermally sublimed at a rate of approximately 1 nm/s. The active area of each solar cell is 0.5 cm^2.This resulted in following solar cell configuration: glass substrate/ITO/PEDOT:PSS/active layer/Al. Photovoltaic devices based on polymer:PCBM active layers with weight ratios of 1:1 and 1:2 have been prepared and optimized by variation of solution concentration and film thickness. However, the reported efficiencies may not strictly constitute the maximum attainable ones. Figure 6 shows the IV curves of the solar cells based on polymer:PCBM (1:2) active layers. For illumination a solar simulator (AM1.5, class A) was used.

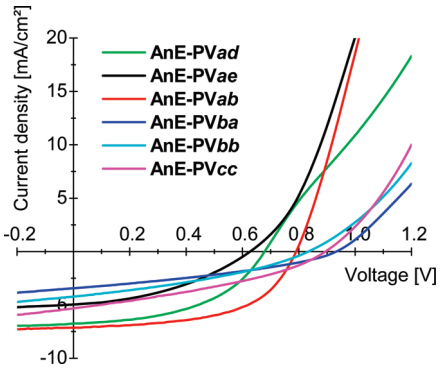

Figure 6. Comparison between the light IV-curves for all materials investigated in 1:2 blends with PCBM.

Table 6 summarizes the photovoltaic parameters obtained from current−voltage (*IV*) measurements for all polymer:PCBM blends. These include the short circuit current, J_{SC}, the open circuit voltage, V_{OC}, the fill factor, FF, the series and parallel resistance, R_S and R_P, respectively.

In general higher energy conversion efficiencies, η, were obtained for solar cells with active layers having higher fullerene contents. The energy conversion efficiencies range from η = 0.34% to 3.14%. The lowest energy conversion efficiencies were obtained for the amorphous polymers **AnE-PV*ba*** and ***-bb***, despite their highest mobility, due to high miscibility of the active layer components resulting in resulting in insufficient percolation paths for the photogenerated charges.

Among the polymer exhibiting a good percolation path due to their more coarse grained thin film nanomorphology, **AnE-PV*ab*** shows the highest energy conversion efficiency. It is the polymer with the highest $\pi-\pi$-stacking distance $d_{\pi\pi}$ = 0.386 nm of all polymers in this series. Higher side chain density in **AnE-PV*ad*** and ***-ae*** leads to increased resistance against charge transfer between donor and acceptor, resulting in lower photovoltages and fill factors and thus lower photovoltaic performance as compared to **AnE-PV*ab***.

Table 6. Summary of the Photovoltaic Parameters of the Polymer Solar Cells[b]

AnE-PV*i*:PCBM (blend ratio)	J_{SC} (mA/cm^2)	V_{oc} (V)	FF (%)	η (%)	R_S (Ω)	R_P (Ω)
ad:PCBM (1:1)	5.66	0.65	41.33	1.52	40.7	1106
ad:PCBM (1:2)	6.75	0.68	48.37	2.22	23	1443
ae:PCBM (1:1)	4.22	0.64	40.03	1.08	37.8	1058
ae:PCBM (1:2)	4.97	0.62	39.82	1.23	20.9	1064
ab:PCBM (1:1)	6.13	0.81	49.08	2.44	22.2	1480
ab:PCBM (1:2)	7.14	0.79	55.65	3.14	14.3	2227
cc:PCBM (1:1)	3.66	0.93	29.98	1.02	36.3	657
cc:PCBM (1:2)	5.65	0.91	36.9	1.90	19.1	606
cc:PCBM (1:1)[a]	5.86	0.91	37.5	2.00	12.8	625
ba:PCBM (1:1)	1.59	0.77	27.38	0.34	18.6	1081
ba:PCBM (1:2)	3.44	0.93	34.67	1.11	31.2	942
bb:PCBM (1:1)	1.99	0.84	29.23	0.49	16	1012
bb:PCBM (1:2)	4.22	0.83	34.8	1.22	26.6	740

[a]Active layer spin-cast from a mixture of chloroform and chlorobenzene. [b]The active layer (area of 0.5 cm^2) was spin-cast from chlorobenzene solution.

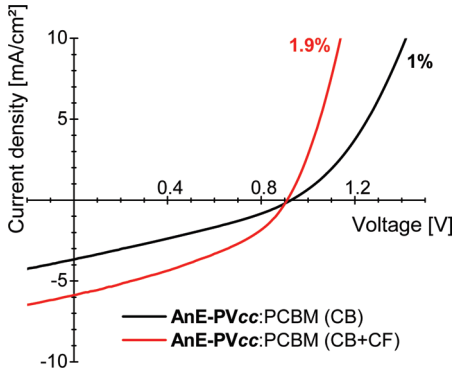

Figure 7. Comparison of light IV−curves for **AnE-PV*cc***:PCBM (1:1) blends cast from chlorobenzene (CB) and a chlorobenzene−chloroform (1:1) mixture (CB + CF), respectively. The latter shows a increased power conversion efficiency.

Thus, and in accordance to our previous results on the effect of the side chains on the photovoltaic performance of PPE−PPV based materials,[8] the open circuit voltage, V_{OC}, increases with decreasing side chain density. For instance, in the case of polymer:PCBM (1:1) blends, polymers bearing longer dodecyloxy (**AnE-PV*ae***) or decyloxy (**AnE-PV*ad***) side groups lead to low V_{OC} values around 0.65 V. Polymers decorated with octyloxy and/or 2-ethylhexyloxy-groups, **AnE-PV*ab***, ***-bb***, ***-ba***, yield V_{OC} values of approximately 0.80 V. Whereas **AnE-PV*cc*** having the lowest side chain density due to grafting of methyloxy groups demonstrates the highest V_{OC} (≈0.90 V). The same trend is observed for 1:2 blends putting aside **AnE-PV*ba***.

The relatively low fill factors, FF, and relatively high series resistances, R_S, in all blends indicate a nonbalanced charge transport i.e. the fullerene content should be increased for further optimization. Only the short circuit currents, J_{SC}, from solar cells based on polymers **AnE-PV*ad***, ***-ab***, and ***-cc*** reach reasonable values between 5 and 7 mA/cm^2, which correspond to more than 50% of what can be expected based on the corresponding absorption spectra.

Especially polymer **AnE-PV*bb*** shows only inferior currents, which may indicate incomplete or hindered charge separation efficiency after transfer. Furthermore, the larger current densities of **AnE-PV*ab*** as compared to **AnE-PV*bb*** may be related to a better ordering caused by $\pi-\pi$-stacking, leading to improved charge transport properties. The high photocurrent densities of photovoltaic devices based on **AnE-PV*cc*** may be related to a lower side-chain density as compared to **AnE-PV*bb***. In general, smaller parallel resistances, R_P, lead to smaller fill factors in case of **AnE-PV*bb*** and **AnE-PV*cc***, while the large photocurrents in case of **AnE-PV*ab*** and **AnE-PV*cc*** promote relatively high power conversion efficiencies of $\eta \geq 2\%$.

A first application of solvent mixtures as a possible way for polymer solar cell optimization was carried out on polymer **AnE-PV*cc***. Changing the solvent from chlorobenzene to a chlorobenzene:chloroform (1:1 volume ratio) mixture for active layer deposition resulted in a 2-fold increase in the power conversion efficiency (see Table 6). Figure 7 compares the IV-curves obtained for the solar cells based on polymer **AnE-PV*cc*** active layers deposited from chlorobenzene and a mixture of chlorobenzene:chloroform, respectively. Detailed studies dealing with solvent mixtures for polymer solar cell optimization are presently going on.

Conclusions

We have synthesized and characterized eight anthracene-containing PPE-PPV copolymers bearing different side chains. We have established a correlation between the ability to form $\pi-\pi$-stacking, the absorption behavior, the charge carrier mobility, the active layer nanoscale morphology, and the photovoltaic performance. The $\pi-\pi$-stacking ability was controlled through grafting of linear and/or branched alkoxy side chains. Polymer with octyloxy substitution close the AnE units (**AnE-PV*ab***, ***-ad***, ***-ae***) arrange in a stacked structure. Whereas asymmetric (**AnE-PV*cc***) or branched side chain substitution (**AnE-PV*bb***, ***-ba***) near the AnE unit yields less organized or even amorphous polymers, respectively. For polymers with strong tendency of stacking well resolved thin film absorption peaks were recorded. The polymers with less or no intrinsic stacking ability exhibit less or no structured absorption peaks. Although they exhibit higher hole mobilities as compared to their ordered counterparts, insufficient donor-acceptor phase separation in these polymers hinders efficient charge separation and, thus leads to poor photovoltaic performance. Stronger phase separation and better photovoltaic performance resulted from polymers inclined to stacking, while the best performance was achieved from **AnE-PV*ab***, exhibiting the highest $d_{\pi\pi}$ value. Solar cells with efficiencies ranging from 0.34 to 3.14% were obtained. It was not possible to include the thin film absolute photoluminescence quantum yield in the correlation due to the broad range of error during the measurements, however the highest absolute Φ_f value of 6% was obtained for **AnE-PV*bb***, bearing solely branched 2-ethylhexyl side chains. An optimization of the solar cells through an increase of the acceptor content as well as by use of solvents mixtures is under way and will be reported in future.

Acknowledgment. D.A.M.E., S.R., and H.H. are grateful to the DFG for financial support in the framework of Priority Program SPP 1355. V.C. acknowledges the financial support of

the Ministry of Education, Youth and Sports of the Czech Republic (Grant No. 1M06031).

Supporting Information Available: Text giving details describing the experimental conditions as well as the synthesis and characterization of the materials, schemes showing the syntheses, and figures showing the TGA curves of the polymers, the cyclic voltamogramm of the polymers, and CELIV timing diagram. This material is available free of charge via the Internet at http://pubs.acs.org.

References and Notes

(1) (a) Brabec, C. J.; Sariciftci, N. S.; Hummelen, C. J. *Adv. Funct. Mater.* **2001**, *11*, 15. (b) Schilinsky, P.; Asawapirom, U.; Scherf, U.; Biele, M.; Brabec, C. J. *Chem. Mater.* **2005**, *17*, 2175. (c) Wong, W.-Y. *Macromol. Chem. Phys.* **2008**, *209*, 14. (d) Krebs, F. C. *Energy Mater.* **2009**, *93*, 394. (e) Chen, L. M.; Hong, Z. R.; Li, G.; Yang, Y. *Adv. Mater.* **2009**, *21*, 1434.

(2) (a) Hoppe, H.; Sariciftci, N. S. *J. Mater. Res.* **2004**, *19*, 1924. (b) Hoppe, H. Sariciftci, N. S. *Polymer Solar Cells in Photoresponsive Polymers II*, Eds.: Marder, S. R. Lee, K. S., Advances in Polymer Science: Springer: Berlin and Heidelberg, Germany, 2008; pp 1−86 (c) Winder, C.; Sariciftci, N. S. *J. Mater. Chem.* **2004**, *14*, 1077. (d) Kroon, R.; Lenes, M.; Hummelen, J. C.; Blom, P. W. M.; de Boer, B. *Polym. Rev.* **2008**, *48*, 531. (d) Cheng, Y.-J.; Yang, S.-H.; Hsu, C.-S. *Chem. Rev.* **2009**, *109*, 5868.

(3) (a) Kim, J. Y.; Lee, K.; Coates, N. S.; Moses, D.; Nguyen, T. Q.; Dante, M.; Heeger, A. J. *Science* **2007**, *317*, 222. (b) Park, S. H.; Roy, A.; Beaupre, S.; Cho, S.; Coates, N.; Moon, J. S.; Moses, D.; Lerclerc, M.; Lee, K.; Heeger, A. J. *Nat. Photonics* **2009**, *3*, 297. (c) Chen, H.-Y.; Hou, J.; Zhang, S.; Liang, Y.; Yang, G.; Yang, Y.; Yu, Li.; Wu, Li.; Li, G. *Nat. Photonics* **2009**, *3*, 649.

(4) (a) Hoppe, H.; Sariciftci, N. S. *J. Mater. Chem.* **2006**, *16*, 45. (b) Hoppe, H. Sariciftci, N. S. *Nanostructure and Nanomorphology Engineering in Polymer Solar Cells in Nanstructured Materials for Solar Energy Conversion*; Soga, T., Eds.; Elsevier: Amsterdam, 2006; p 277.

(5) (a) Shaheen, S. E.; Brabec, C. J.; Sariciftci, N. S.; Padinger, F.; Fromherz, T.; Hummelen, J. C. *Appl. Phys. Lett.* **2001**, *78*, 841. (b) Chirvase, D.; Parisi, J.; Hummelen, J. C.; Dynakov, V. *Nanotechnology* **2004**, *15*, 1317. (c) Erb, T.; Zhokhavets, U.; Gobsch, G.; Raleva, S.; Stühn, B.; Schilinsky, P.; Waldauf, C.; Brabec, C. J. *Adv. Funct. Mater.* **2005**, *15*, 1193. (d) Li, G.; Shrotriya, V.; Huang, J.; Yao, Y.; Moriarty, T.; Emery, K.; Yang, Y. *Nat. Mater.* **2005**, *4*, 864. (e) Zhang, F.; Jespersen, K. G.; Björström, C.; Svensson, M.; Andersson, M. R.; Sundström, V.; Magnusson, K.; Moons, E.; Yartsev, A.; Inganäs, O. *Adv. Funct. Mater.* **2006**, *16*, 667.

(6) (a) Peet, J.; Kim, J. Y.; Coates, N. E.; Ma, W. L.; Moses, D.; Heeger, A. J.; Bazan, G. C. *Nat. Mater.* **2007**, *6*, 497. (b) Cho, S.; Lee, J. K.; Moon, J. S.; Yuen, J.; Lee, K.; Heeger, A. J. *Org. Electron.* **2008**, *9*, 1107.

(7) (a) Bunz, U. H. F. *Chem. Rev.* **2000**, *100*, 1605. (b) Brizius, G.; Pschirer, G. N.; Steffen, W.; Stitzer, K.; zur Loye, H.-C.; Bunz, U. H. F. *J. Am. Chem. Soc.* **2000**, *122*, 12435. (c) Egbe, D. A. M.; Tillmann, H.; Birckner, E.; Klemm, E. *Macromol. Chem. Phys.* **2001**, *202*, 2712. (d) Colak, D. G.; Egbe, D. A. M.; Birckner, E.; Yurteri, S.; Cianga, I.; Tekin, E.; Schubert, U. S.; Yagci, Y. *Eur. Polym. J.* **2009**, *45*, 490.

(8) Egbe, D. A. M.; Nguyen, L. H.; Hoppe, H.; Mühlbacher, D.; Sariciftci, N. S. *Macromol. Rapid Commun.* **2005**, *26*, 1389.

(9) (a) Egbe, D. A. M.; Nguyen, L. H.; Schmidtke, K.; Wild, A.; Günes, S.; Sieber, C.; Sariciftci, N. S. *J. Polym. Sci., Part A: Polym. Chem.* **2007**, *45*, 1619. (b) Egbe, D. A. M.; Carbonnier, B.; Birckner, E.; Grummt, U.-W. *Prog. Polym. Sci.* **2009**, *34*, 1023.

(10) (a) Chen, Z.-K.; Huang, W.; Wang, L. H.; Kang, E. T.; Chen, B. T.; Lee, C. S.; Lee, S. T. *Macromolecules* **2000**, *33*, 9015. (b) Yamamoto, T.; Lee, B. L. *Macromolecules* **2002**, *35*, 2993.

(11) (a) Peng, Z. *Polym. News* **2000**, *25*, 185. (b) Egbe, D. A. M.; Roll, C. P.; Klemm, E. *Des. Monomers Polym.* **2002**, *5*, 245. (c) Egbe, D. A. M.; Roll, C. P.; Birckner, E.; Grummt, U.-W.; Stockmann, R.; Klemm, E. *Macromolecules* **2002**, *35*, 3825.

(12) Weder, C.; Wrighton, M. S.; Spreiter, R.; Bosshard, C.; Günther, P. *J. Phys. Chem.* **1996**, *100*, 18931.

(13) (a) Egbe, D. A. M.; Bader, C.; Nowotny, J.; Günther, W.; Klemm, E. *Macromolecules* **2003**, *36*, 5459. (b) Wild, A.; Egbe, D. A. M.; Birckner, E.; Cimrova, V.; Baumann, R.; Grummt, U.-W.; Schubert, U. S. *J. Polym. Sci., Part A: Polym. Chem.* **2009**, *47*, 2243.

(14) (a) Hoppe, H.; Egbe, D. A. M.; Mühlbacher, D.; Sariciftci, N. S. *J. Mater. Chem.* **2004**, *14*, 3462. (b) Hoppe, H.; Sariciftci, N. S.; Egbe, D. A. M.; Mühlbacher, D.; Koppe, M. *Mol. Cryst. Liq. Cryst.* **2005**, *426*, 255.

(15) Kietzke, T.; Shin, R. Y. C.; Egbe, D. A. M.; Chen, Z.-K.; Sellinger, A. *Macromolecules* **2007**, *40*, 4424.

(16) (a) Carbonnier, B.; Egbe, D. A. M.; Birckner, E.; Grummt, U.-W.; Pakula, T. *Macromolecules* **2005**, *38*, 7546. (b) Rathgeber, S.; Bastos de Toledo, D.; Birckner, E.; Hoppe, H.; Egbe, D. A. M. *Macromolecules* **2009**, DOI:10.1021/ma902132c.

(17) Egbe, D. A. M.; Carbonnier, B.; Ding, L.; Mühlbacher, D.; Eckhard, B.; Pakula, T.; Karasz, F. E.; Grummt, U.-W. *Macromolecules* **2004**, *37*, 7451.

(18) Egbe, D. A. M.; Carbonnier, B.; Paul, E. L.; Mühlbacher, D.; Kietzke, T.; Birckner, E.; Neher, D.; Grummt, U.-W.; Pakula, T. *Macromolecules* **2005**, *38*, 6269.

(19) Carbonnier, B.; Pakula, T.; Egbe, D. A. M. *J. Mater. Chem.* **2005**, *15*, 880.

(20) Egbe, D. A. M.; Sell, S.; Ulbricht, C.; Birckner, E.; Grummt, U.-W. *Macromol. Chem. Phys.* **2004**, *205*, 2105.

(21) (a) Garay, R. O.; Naarmann, H.; Müllen, K. *Macromolecules* **1994**, *27*, 1922. (b) Mikroyannidis, J. A.; Stylianakis, M. M.; Balraju, P.; Suresh, P.; Sharma, G. D. *Appl. Mater. Interfaces* **2009**, *1*, 1711.

(22) (a) McGehee, M. D.; Heeger, A. J. *Adv. Mater.* **2000**, *12*, 1655. (b) Nguyen, T.; Doan, V.; Schwartz, B. J. *J. Chem. Phys.* **1999**, *110*, 4068.

(23) Bässler, H. *Phys. Status Solidi B* **1981**, *107*, 9.

(24) Borsenberger, P. M.; Wiss, D. S. *Organic Photoreceptor for Imaging Systems*; Marcel Dekker: New York, 1993.

(25) Osterbacka, R.; Pivrikas, A.; Juska, G.; Genevicius, K.; Arlauskas, K.; Stubb, H. *Curr. Appl. Phys.* **2004**, *4*, 534.

(26) Tiedje, T.; Rose, A. *Solid State Commun.* **1981**, *37*, 49.

(27) Juska, G.; Genevicius, K.; Arlauskas, K.; Osterbacka, R.; Stubb, H. *Phys. Rev. B* **2002**, *65*, 233208.

(28) Horowitz, G. *Adv. Mater.* **1998**, *10*, 365.

(29) Klauk, H.; Schmid, G.; Radlik, W.; Weber, W.; Zhou, L.; Sheraw, C. D.; Nichols, J. A.; Jackson, T. N. *Solid-State Electron.* **2003**, *47*, 297.

(30) Juška, G.; Arlauskas, K.; Viliūnas, M.; Kočka, J. *Phys. Rev. Lett.* **2000**, *84*, 4946.

(31) McCulloch, I.; Heeney, M.; Chabinyc, M. L.; DeLongchamp, D.; Kline, R. J.; Cölle, M.; Duffy, W.; Fischer, D.; Gundlach, D.; Hamadani, B.; Hamilton, R.; Richter, L.; Salleo, A.; Shkunov, M.; Sparowe, D.; Tierney, S.; Zhang, W. *Adv. Mater.* **2009**, *21*, 1091.